Selective probing of hidden spin-polarized states in inversion-symmetric bulk MoS_2

E. Razzoli,[1,*] T. Jaouen,[1] M.-L. Mottas,[1] B. Hildebrand,[1] G. Monney,[1] A. Pisoni,[2] S. Muff,[3,4] M. Fanciulli,[3,4] N. C. Plumb,[3] V. A. Rogalev,[3] V. N. Strocov,[3] J. Mesot,[3,4] M. Shi,[3] J. H. Dil,[3,4] H. Beck,[1] and P. Aebi[1]

[1]*Département de Physique and Fribourg Center for Nanomaterials, Université de Fribourg, CH-1700 Fribourg, Switzerland*

[2]*Laboratory of Physics of Complex Matter, Ecole Polytechnique Fédérale de Lausanne, CH-1015 Lausanne, Switzerland*

[3]*Swiss Light Source, Paul Scherrer Institute, CH-5232 Villigen PSI, Switzerland*

[4]*Institute of Physics, École Polytechnique Fédérale de Lausanne, CH-1015 Lausanne, Switzerland*

(Dated: January 26, 2017)

Spin- and angle-resolved photoemission spectroscopy is used to reveal that a large spin polarization is observable in the bulk centrosymmetric transition metal dichalcogenide MoS_2. It is found that the measured spin polarization can be reversed by changing the handedness of incident circularly-polarized light. Calculations based on a three-step model of photoemission show that the valley and layer-locked spin-polarized electronic states can be selectively addressed by circularly-polarized light, therefore providing a novel route to probe these hidden spin-polarized states in inversion-symmetric systems as predicted by Zhang *et al.* [Nature Physics **10**, 387 (2014)].

arXiv:1701.07109v1 [cond-mat.mtrl-sci] 24 Jan 2017

Transition metal dichalcogenide (TMDC) monolayers have been heavily investigated due to the locking of the spin with valley pseudospins and the presence of a direct gap, which makes them ideal candidates for valleytronic devices [1]. Thanks to the lack of inversion symmetry and the non-negligible spin-orbit coupling, TMDC monolayers also feature well-defined spin-polarized ground states [2], which can in principle be investigated by spin- and angle-resolved photoemission spectroscopy (spin-ARPES). However, while few ARPES studies clearly observed the indirect to direct band gap transition going from the bulk crystal to the monolayer [3–6], spin-ARPES investigation of TMDC monolayers is more challenging, given the low cross-section of photoemission from single layers.

ARPES measurements on the bulk system are instead less demanding but early studies detected spin-resolved signals only from TMDCs with broken inversion symmetry [7]. Interestingly, a recent theoretical study [8] suggested that the spin texture of the TMDC could be probed by photoemission, even in the inversion symmetric bulk TMDC crystals, as a result of the localization of two spin-degenerated valence band maxima on different layers of the unit cell and of the finite penetration depth of the photoemission process probing preferentially the uppermost layer. Experimentally this effect has been observed for WSe_2 where the spin orbit (SO) coupling is the strongest one among the TMDCs [9].

Here we show that a large out-of-plane spin-polarization is observable in the bulk dichalcogenide MoS_2, and more importantly, that its sign depends on the handedness of the incident circularly-polarized light. Our calculations, based on a three step model of the photoemission process demonstrate that the observed spin reversal is an initial state effect. Using left (C_L) and right-handed (C_R) circularly-polarized light results in selecting different initial states that present a positive or negative out-of-plane spin polarization depending on their localization on the S-Mo-S layers of the $2H$-stacked MoS_2 unit cell. Our findings not only highlight the locking of the spin with layer and valley pseudospins in MoS_2 but also provide a novel and improved route, other than taking profit of the inelastic mean free path (IMFP) [8], for selectively probing hidden spin-polarized bands in inversion symmetric systems.

The soft x-ray ARPES and spin-ARPES experiments were respectively performed at the ADRESS beamline [10] and at the COPHEE end-station of SIS beamline at the Swiss Light Source, Paul Scherrer Institut, Villigen, Switzerland. Base pressures were better than 4×10^{-10} mbar, with a sample temperature of ∼25 K [11]. The chemical vapor transport-grown $2H$-MoS_2 crystal consisting of hexagonal $2H$-stacked S-Mo-S layers separated by a van der Waals gap (Fig. 1(a) [18]), has been cleaved *in-situ* at low temperature. Figure 1(b) (top panel) shows the ARPES intensity plot of bulk MoS_2 along the $\overline{K}$-$\overline{\Gamma}$ high-symmetry direction of the Brillouin zone [bottom of Fig. 1(a)] and measured using circularly-polarized light with an overall energy resolution of 50-80 meV. The observed bands are in agreement with previous ARPES measurements [3, 5, 20], with the top of the valence band at $\overline{\Gamma}$ originating from Mo d_{z^2}/p_z orbitals and that lies ∼600 and ∼800 meV above the upper (VB1) and lower (VB2) valence bands at $\overline{K}$ with mainly Mo $d_{x^2-y^2}$, d_{xy} orbital characters. The observed dispersion is in good agreement with our density functional theory (DFT) calculation within the local density approximation (LDA) between Γ and K, given the small k_z-dispersion along $K-H$ direction (see Fig. 1(b) bottom panel) [11].

Figures 1 (c)-(e) present the experimental spin-ARPES intensities (top) and the spin-polarization energy distribution curves (bottom) at the $\overline{K}$ point along the three spatial coordinates x, y, and z in the sample frame measuring in-plane (P_x, P_y), and out-of-plane (P_z) spin polarization. Conversion from the coordinate system given by the Mott polarimeters to the sample frame is per-

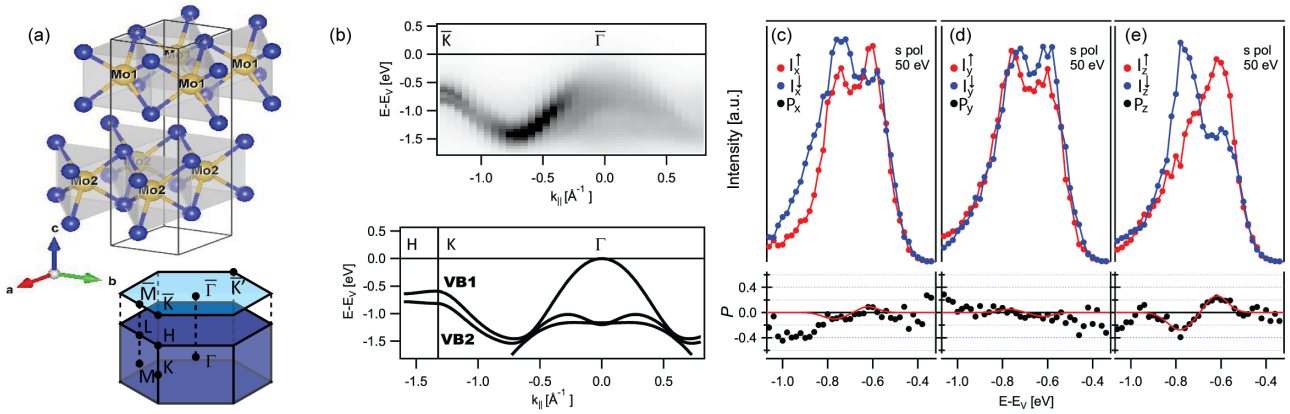

FIG. 1: (a) Structural model (top) and Brillouin zone (bottom) of $2H$-MoS_2. (b) ARPES intensity map along $\overline{K}-\overline{\Gamma}$ direction (top), and DFT-LDA calculated band structure showing the band dispersion along $K-\Gamma$ and $H-K$ directions (bottom). (c)-(d) Spin-resolved intensities (top) and spin polarization curves (bottom) at the $\overline{K}$-point along x, y, and z, respectively. Continuous red lines in the bottom panels are Gaussian fits, resulting in $P_x = \mp 0.08$, $P_y = \pm 0.05$ and $P_z = \mp 0.28$. Spin-ARPES data were acquired at $h\nu = 50$ eV with $s-$polarized light.

formed according to [19]. The difference in binding energy between VB1 and VB2 is 170 meV, in agreement with previous studies [20]. The measured spin polarization is almost entirely out-of-plane with a negligible small in-plane component. The measured out-of-plane spin polarization points upwards and downwards for the upper and lower valence band, respectively, similarly to what has been observed in WSe_2 [9].

The z-component of the spin polarization displays an interesting polarization dependence [Fig. 2]. The spin polarization measured with p- [Fig. 2 (a)], and C_L polarization [Fig. 2 (b)] are in agreement with the observation with s-polarized light [Fig. 1 (e)], with the only difference of an increasing absolute value of the spin polarization fraction. Instead, when probed with C_R light the out-of-plane spin polarization changes its sign, i.e., the z-component of the detected photo-electron points upwards and downwards for the lower and upper valence band, respectively [Fig. 2 (c)]. Interestingly, the light handedness-induced reversal of the z-component is also observable at other photon-energy [e.g. at $h\nu = 58$ eV as shown in Fig. 2 (d)-(e)], therefore indicating that it does not depend on the three-dimensional (k_z) band dispersion.

A possible explanation of our observation would be that photoelectron spin flips during the photoemission process, i.e., we observed a final state matrix element effect. Up to now, most of spin-ARPES studies dealing with k-resolved light-induced spin rotations have been carried out on topological insulators (TI), due to the large strength of the SO-coupling and to the high quality of the ARPES data in such systems [21–24]. It has been experimentally shown that light-induced spin rotations are observable only at low photon energy (about 6 eV) [21, 24]. Theoretically it has been suggested that the SO-induced term in the light-matter interaction Hamiltonian H_{SO}^{int} [25] is responsible for the spin events tuned by light polarization. However, in contrast to the TI that exhibit extremely large SO-coupling, in TMDCs and especially in MoS_2 [5], the $\langle i|H_{SO}^{int}|f\rangle$ term can be neglected and the observed flip in the out-of-plane spin-polarization has to be related to a different mechanism [11].

Instead, the origin of the sign inversion of P_z can be understood analyzing the idealized case of a TMDC bilayer with small interlayer coupling $t_\perp$. In this simplified model, the top of the valence band VB1 ($E_b = E_1$) at K is doubly degenerate and originates in Mo $d_{x^2-y^2}$, d_{xy} orbitals. The eigenstates expressed in terms of spherical harmonics $|l,m\rangle_\mu$ are then given by [11, 26]:

$$\begin{aligned} |1,E_1\rangle &= \frac{\cos\alpha\,|2,2\rangle_1 + \sin\alpha\,|2,-2\rangle_2}{\sqrt{2}}\,|\uparrow\rangle \\ |2,E_1\rangle &= \frac{\sin\alpha\,|2,2\rangle_1 + \cos\alpha\,|2,-2\rangle_2}{\sqrt{2}}\,|\downarrow\rangle \end{aligned} \tag{1}$$

using $\mu = 1(2)$ for the upper (lower) Mo layer of the $2H$-stacked MoS_2 unit cell [Fig. 3(a)], and with $\cos 2\alpha = \lambda_{so}/\sqrt{\lambda_{so}^2 + t_\perp^2}$ that corresponds to the spin-dependent layer polarization of the holes states. The spin-valley coupling of holes in monolayers λ_{so} is calculated to be 1.7 times higher than the interlayer hopping $t_\perp$ in MoS_2 [26], therefore resulting in a substantial layer-dependent spin-polarization ($\cos 2\alpha = 0.863$).

The states $|1,E_1\rangle$ and $|2,E_1\rangle$ respectively contribute to the spin-up ($I_{\uparrow,z}^{\boldsymbol{\epsilon}}$) and spin-down ($I_{\downarrow,z}^{\boldsymbol{\epsilon}}$) intensity [11]:

$$\begin{aligned} I_{\uparrow,z}^{\boldsymbol{\epsilon}} &\propto |\cos(\alpha)\boldsymbol{\kappa}_{2,2}\cdot\boldsymbol{\epsilon} + \sin(\alpha)\delta e^{-i\mathbf{k}\cdot\mathbf{d}_l}\boldsymbol{\kappa}_{2,-2}\cdot\boldsymbol{\epsilon}|^2 \\ I_{\downarrow,z}^{\boldsymbol{\epsilon}} &\propto |\sin(\alpha)\boldsymbol{\kappa}_{2,2}\cdot\boldsymbol{\epsilon} + \cos(\alpha)\delta e^{-i\mathbf{k}\cdot\mathbf{d}_l}\boldsymbol{\kappa}_{2,-2}\cdot\boldsymbol{\epsilon}|^2 \end{aligned} \tag{2}$$

with $\boldsymbol{\kappa}_{l,m} = \langle e^{i\mathbf{k}\cdot\mathbf{r}}|\mathbf{r}|l,m\rangle$, $\mathbf{d}_l = (\frac{1}{2}a, \frac{2}{3}a, -\frac{1}{2}c)$ the relative atomic displacement between the upper and lower Mo

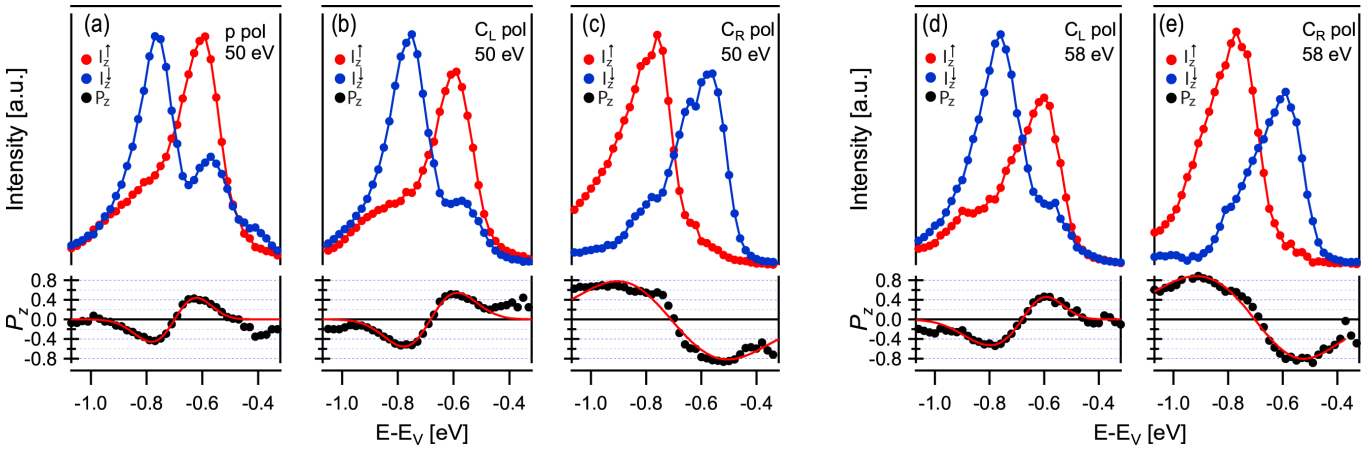

FIG. 2: Spin-ARPES data acquired at $h\nu = 50$ and $h\nu = 58$ eV. (a)-(c) Spin-resolved intensities (top) and spin polarization curves (bottom) along z at the $\overline{K}$-point acquired with p, C_L and C_R polarization, respectively ($h\nu = 50$ eV). (d), (e) Spin-resolved intensities (top) and spin polarization curves (bottom) at the $\overline{K}$-point acquired with C_L and C_R polarization, and $h\nu = 58$ eV. Continuous red lines in the bottom panels are Gaussian fits, resulting in $P_z(p, 50\text{ eV}) = \mp 0.50$, $P_z(C_L, 50\text{ eV}) = \mp 0.68$, $P_z(C_R, 50\text{ eV}) = \pm 0.85$, $P_z(C_L, 58\text{ eV}) = \mp 0.54$, and $P_z(C_R, 58\text{ eV}) = \pm 0.91$.

layers, $\boldsymbol{\epsilon}$ the light polarization vector, and $\delta = e^{-\frac{c}{2\lambda_e}}$, an attenuation factor that takes into account the photoelectrons IMFP λ_e. For normal incident circularly-polarized light the conservation of the total angular momentum dictates that only the states with $m_k = m \pm 1$, can give a non-vanishing contribution to $\boldsymbol{\kappa}_{l,m}$, once the free-electron final state is decomposed in spherical harmonics $|e^{i\mathbf{k}\cdot\mathbf{r}}\rangle = \sum_{l_k,m_k} d_{l_k,m_k}(\mathbf{k}, r)\,|l_k, m_k\rangle$.

In Fig. 3 we illustrate the dipole-allowed transitions for the eigenstate of VB1 at the K point, for the case of vanishing interlayer coupling ($\alpha = 0$). In this case spin up and spin down states are fully locked on the upper and lower S-Mo-S layer, respectively [Fig. 3(a)].

For C_L light [Fig. 3(b), left-hand-side], the available final states have $m_k = m - 1$, and are $\{|1,1\rangle, |3,1\rangle\}$ for $m = 2$ and $\{|3,-3\rangle\}$ for $m = -2$. As expected from the higher number of final states available for a dipole transition from a state with $m = 2$, our numerical evaluation shows that the cross-section for transition to the states $\{|1,1\rangle, |3,1\rangle\}$ is one order of magnitude larger than to $\{|3,-3\rangle\}$, i.e., $|\boldsymbol{\kappa}_{2,2}\cdot\boldsymbol{\epsilon}^{\mathbf{n}}_{C_L}|/|\boldsymbol{\kappa}_{2,-2}\cdot\boldsymbol{\epsilon}^{\mathbf{n}}_{C_L}| \approx 10$ [11]. Similarly and according to the relation $\boldsymbol{\kappa}_{l,\pm m}\cdot\boldsymbol{\epsilon}_{C_{R/L}} = \boldsymbol{\kappa}_{l,\mp m}\cdot\boldsymbol{\epsilon}_{C_{L/R}}$, the available final states of a dipole transition induced by C_R light [Fig. 3(b) right-hand-side], have $m_k = m + 1$ and $|\boldsymbol{\kappa}_{2,-2}\cdot\boldsymbol{\epsilon}^{\mathbf{n}}_{C_R}|/|\boldsymbol{\kappa}_{2,2}\cdot\boldsymbol{\epsilon}^{\mathbf{n}}_{C_R}| \approx 10$. For a non-zero interlayer hopping, eq. (2) thus gives:

$$P_z^{C^{\mathbf{n}}_{R/L}} = \frac{I^{\boldsymbol{\epsilon}^{\mathbf{n}}_{C_{R/L}}}_{\uparrow,z} - I^{\boldsymbol{\epsilon}^{\mathbf{n}}_{C_{R/L}}}_{\downarrow,z}}{I^{\boldsymbol{\epsilon}^{\mathbf{n}}_{C_{R/L}}}_{\uparrow,z} + I^{\boldsymbol{\epsilon}^{\mathbf{n}}_{C_{R/L}}}_{\downarrow,z}} \approx \mp\cos 2\alpha. \qquad (3)$$

This demonstrates that the layer-locked, hidden spin-polarized states of the K valley can be probed through the spin-dependent selection rules introduced by the use of circularly-polarized light. This not only selects which hidden-spin polarized state will be observed, but also overcomes the IMFP-limited probing of the spin texture of the uppermost layer as introduced by using linearly-polarized light [8, 9, 27, 28].

This interpretation is confirmed by calculating the spin-resolved ARPES intensity and the spin polarization for 8 MoS_2 layers as a function of both, the light geometry and polarization and using the spin doublet of the topmost VB (VB1) in valley K as the initial state [11]. The spin up (down) state is highly localized on the odd

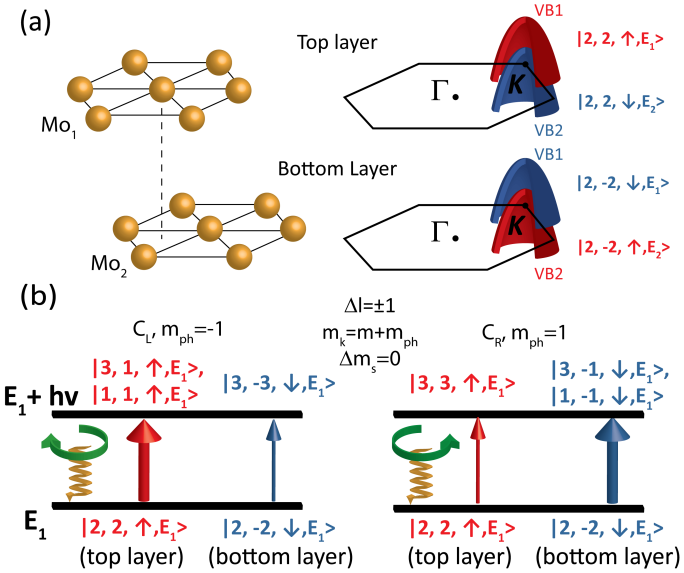

FIG. 3: (a) Schematic of the layer-resolved band dispersion of VB1 and VB2 around the K point. (b) Dipole-allowed transitions for the eigenstate of VB1 for vanishing interlayer coupling ($\alpha = 0$) at the K point.

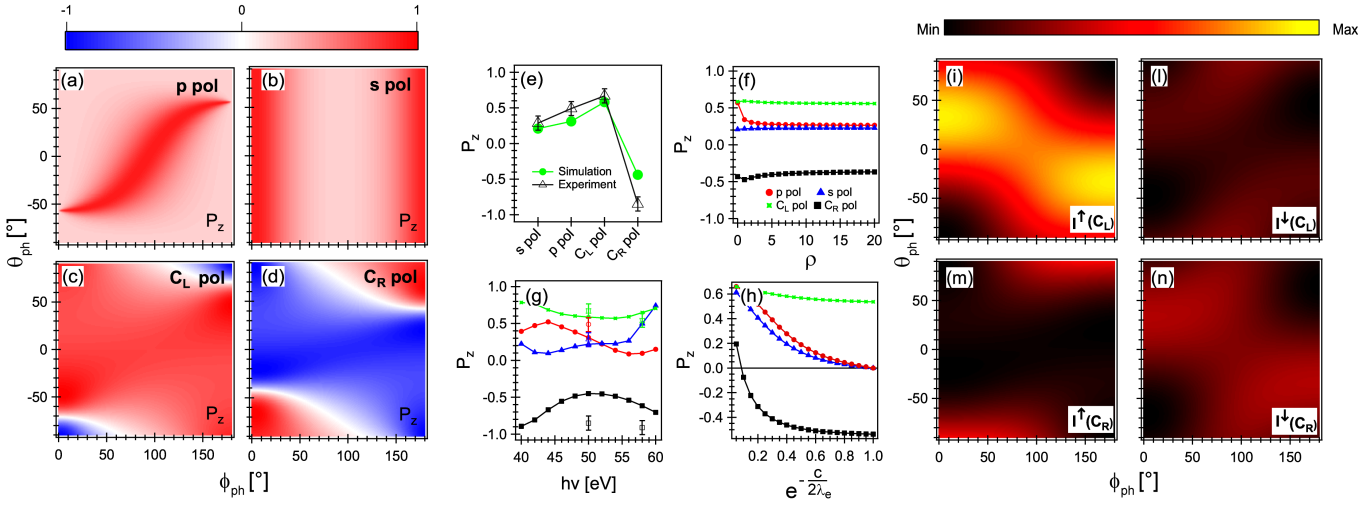

FIG. 4: Three-step model photoemission calculations. (a)-(d) Spin polarization (P_z) maps for p, s, C_L and C_R polarization, respectively ($h\nu = 50$ eV). (e) Experimental and simulated spin polarization along z. (f)-(h) radial integral (ρ), photon energy ($h\nu$) and IMFP (λ_e)-dependence of P_z, respectively. Empty symbols in (g) show the experimental P_z from Fig. 2 (a)-(e). (i)-(n) Spin-resolved intensity maps for C_L (top panels) and C_R (bottom panels) polarized light.

(even) Mo layer, in analogy to the bilayer model and λ_e, included following the methods proposed by [22, 23], has been fixed to the interlayer distance (6.1 Å).

The spin polarization intensity maps as a function of the incoming light geometry and polarization [Fig. 4 (a)-(d)] [29], show that for $s-$ and p-polarized light the z-component of the spin is positive irrespective of the geometry, in agreement with our experimental observations and with what is expected in MoS_2 as the result of the finite probing depth of the photoemission process [8, 9]. Our model further predicts positive and negative spin polarization for C_L and C_R-polarized lights for most of the possible experimental geometries, including ours ($\theta_{ph} = 48.3°$ and $\phi_{ph} = 71°$), as well as sign inversion for extreme geometries corresponding to grazing incidence of the radiation [Fig. 4 (c), (d)].

Overall, the theoretical P_z values obtained for the various light polarization and corresponding to our geometry agree well with the experimental data as shown in Fig. 4 (e). The weak dependence of the spin-polarization on the radial integral of the overlap between the initial and the final state (ρ) indicates that the calculations are not strongly dependent on the numerical details of the chosen states [Fig. 4 (f)], and the observed spin-flip is predicted to be robust against changes in the photon energy [Fig. 4 (g)], as experimentally observed [Fig. 2 (b)-(e)]. The dependence of the calculated P_z on λ_e [Fig. 4 (h)] also confirms that using circularly-polarized light allows overcoming the IMFP limitation in variance with the case of linearly polarized lights where a presence of a small λ_e is essential for observing any spin polarization. Finally, the spin-resolved intensity maps in Fig. 4 (i)-(n) account for the selective ability of the circularly-polarized light to probe the layer-locked spin-polarized states for most of the possible light geometries. As the result of the finite λ_e at $h\nu = 50$ eV, they also show higher ARPES intensities for C_L than for C_R [Fig. 4 (i), (n) and (l), (m)], with a theoretical $I^{\uparrow}(C_L)/I^{\downarrow}(C_R)$ ratio of 2.65, in close agreement with the experimental value of 2.1 [30].

We finally note that putative interference effects between distinct degenerate initial states [31] and/or small correction to eq.(1), resulting from possible modification within the MoS_2 monolayer, such as mirror symmetry breaking and VB1-VB2 intervalence mixing, might contribute to the spin-polarization. In bulk TMDCs, these contributions only slightly change P_z but may substantially affect the in-plane spin-polarization ($P_{\parallel}$) [11]. Similar to previous studies [9], we observe a small $P_{\parallel}$ [Fig. 1 (c)-(d)], which becomes more sizeable with other polarization [11]. For supported TMDC layers the interaction with the substrate may in some cases enhance these effects whose contributions to both P_z and $P_{\parallel}$ might become more important [32].

In conclusion our ARPES and spin-ARPES measurements of bulk centrosymmetric $2H$-MoS_2 have revealed a large out-of-plane spin-polarization with sign depending on the handedness of incident circularly-polarized light. Our calculations, based on a three-step model of the photoemission process demonstrate that this relates to an initial-state effect of photoemission through the dipole selection rules that allow to intimately probe the valley and layer spin texture of the electronic states. Our finding provides a novel route for studying hidden spin-polarized bands of inversion symmetric systems in laser- or soft x-ray-ARPES where the inelastic mean free path of photoelectrons is typically large.

We acknowledge F. Boschini, M. Michiardi and A. Damascelli for valuable discussions. This project

was supported by the Fonds National Suisse pour la Recherche Scientifique through Div. II. E.R. acknowledges support from the Swiss National Science Foundation (SNSF) grant no. P300P2_164649.

* Corresponding Author: elia.razzoli@unifr.ch;
Present address: Quantum Matter Institute, Department of Physics and Astronomy, University of British Columbia, Vancouver, British Columbia V6T 1Z1, Canada

[1] K. F. Mak, and J. Shan, *Photonics and optoelectronics of 2D semiconductor transition metal dichalcogenides*, Nat. Phot. **10**, 216226 (2016).

[2] D. Xiao, G.-B. Liu, W. Feng,Xiaodong Xu, and W. Yao, *Coupled Spin and Valley Physics in Monolayers of MoS_2 and Other Group-VI Dichalcogenides*, Phys. Rev. Lett. **108**, 196802 (2012).

[3] W. Jin, P-C Yeh, N. Zaki, D. Zhang, J. T. Sadowski, A. Al-Mahboob, A. M. van der Zande, D. A. Chenet, J. I. Dadap, I. P. Herman, P. Sutter, J. Hone, and R. M. Osgood, *Direct Measurement of the Thickness-Dependent Electronic Band Structure of MoS_2 Using Angle-Resolved Photoemission Spectroscopy* Phys. Rev. Lett. **111**, 106801 (2013).

[4] Y. Zhang, T.-R. Chang, B. Zhou, Y.-T. Cui, H. Yan, Z. Liu, F. Schmitt, J. Lee, R. Moore, Y. Chen, H. Lin, H.-T. Jeng, S.-K. Mo, Z. Hussain, A. Bansil, and Z.-X. Shen, *Direct observation of the transition from indirect to direct bandgap in atomically thin epitaxial $MoSe_2$*, Nat. Nanotechnol., **9** , 111 (2014).

[5] T. Eknapakul, P. D. C. King, M. Asakawa, P. Buaphet, R.-H. He, S.-K. Mo, H. Takagi, K. M. Shen,F. Baumberger, T. Sasagawa, S. Jungthawan, and W. Meevasana, *Electronic Structure of a Quasi-Freestanding MoS2 Monolayer* Nano Lett. **14**, 13121316 (2014).

[6] N Alidoust, G. Bian, S.-Y. Xu, R. Sankar, M. Neupane, C. Liu, I. Belopolski, D.-X. Qu, J. D. Denlinger, F.-C. Chou, and M. Z. Hasan, *Observation of monolayer valence band spin-orbit effect and induced quantum well states in MoX_2* Nature Commun. **5**, 4673 (2014).

[7] R. Suzuki, M. Sakano,Y. J. Zhang, , R. Akashi, D. Morikawa, A. Harasawa, K. Yaji, K. Kuroda, K. Miyamoto, T. Okuda, K. Ishizaka, R. Arita, and Y. Iwasa, *Valley-dependent spin polarization in bulk MoS_2 with broken inversion symmetry*, Nat. Nanotech., **9**, 611 (2014).

[8] X. Zhang, Q. Liu, J.-W. Luo, A. J. Freeman and A. Zunger, *Hidden spin polarization in inversion-symmetric bulk crystals* Nature Physics **10**, 387 (2014).

[9] J. M. Riley, F. Mazzola, M. Dendzik, M. Michiardi, T. Takayama, L. Bawden, C. Granerd, M. Leandersson, T. Balasubramanian, M. Hoesch, T. K. Kim, H. Takagi, W. Meevasana, Ph. Hofmann, M. S. Bahramy, J. W. Wells and P. D. C. King, *Direct observation of spin-polarized bulk bands in an inversion-symmetric semiconductor* Nature Physics **10**, 835 (2014).

[10] V.N. Strocov, X. Wang, M. Shi, M. Kobayashi, J. Krempasky, C. Hess, T. Schmitt and L. Patthey, *Soft-X-ray ARPES facility at the ADRESS beamline of the SLS: Concepts, technical realisation and scientific applications*, J. Synchrotron Rad. 21 (2014) 32.

[11] See Supplemental Material [url], which includes Refs. [12–17]

[12] A. Kuc, N. Zibouche, and T. Heine, *Influence of quantum confinement on the electronic structure of the transition metal sulfide TS_2*, Phys. Rev. B **83**, 245213 (2011).

[13] M. Hoesch, T. Greber, V.N. Petrov, M. Muntwiler, M. Hengsberger, W. Auwarter, J. Osterwalder, *Spin-polarized Fermi surface mapping*, Journal of Electron Spectroscopy and Related Phenomena **124** (2002) 263279.

[14] P. Blaha, K. Schwarz, G. Madsen, D. Kvasnicka and J. Luitz, WIEN2k, *An Augmented Plane Wave + Local Orbitals Program for Calculating Crystal Properties* (Karlheinz Schwarz, Techn. Universität Wien, Austria), 2001. ISBN 3-9501031-1-2

[15] G.-B. Liu, W.-Y. Shan, Y. Yao, W. Yao, and D. Xiao, *Three-band tight-binding model for monolayers of group-VIB transition metal dichalcogenides*, Phys. Rev. B **88**, 085433 (2013).

[16] F. Meier, V. Petrov, H. Mirhosseini , L. Patthey, J. Henk, J. Osterwalder and H. J. Dil, *Interference of spin states in photoemission from Sb/Ag(111) surface alloys*, J. Phys.: Condens. Matter **23** 072207 (2011).

[17] M. Hamzavi, M. Movahedi, K.-E. Thylwe and A. A. Rajabi, *Approximate Analytical Solution of the Yukawa Potential with Arbitrary Angular Momenta*, Chin. Phys. Lett. **29**, 080302 (2012).

[18] K. Momma and F. Izumi. *VESTA 3 for three-dimensional visualization of crystal, volumetric and morphology data.* Journal of Applied Crystallography, **44**(6):12721276, December 201.

[19] F. Meier, H. Dil, J. Lobo-Checa, L. Patthey, and J. Osterwalder *Quantitative vectorial spin analysis in angle-resolved photoemission: Bi/Ag(111) and Pb/Ag(111)*, Phys. Rev. B **77**, 165431 (2008).

[20] D. W. Latzke, W. Zhang, A. Suslu, T.-R. Chang, H. Lin, H.-T. Jeng, S. Tongay, J. Wu, A. Bansil, and A. Lanzara, *Electronic structure, spin-orbit coupling, and interlayer interaction in bulk MoS_2 and WS_2* Phys. Rev. B **91**, 235202 (2015).

[21] C. Jozwiak, C-H. Park, K. Gotlieb, C. Hwang, D-H. Lee, S. G. Louie, J. D. Denlinger, C. R. Rotundu, R. J. Birgeneau, Z. Hussain, and A. Lanzara *Photoelectron spin-flipping and texture manipulation in a topological insulator*, Nature Physics **9**, 293298 (2013).

[22] Z.-H. Zhu, C. N. Veenstra, G. Levy, A. Ubaldini, P. Syers, N. P. Butch, J. Paglione, M. W. Haverkort, I. S. Elfimov, and A. Damascelli *Layer-by-Layer Entangled Spin-Orbital Texture of the Topological Surface State in Bi_2Se_3* Phys. Rev. Lett. **110**, 216401 (2013).

[23] Z.-H. Zhu, C.N. Veenstra, S. Zhdanovich, M.P. Schneider, T. Okuda, K. Miyamoto, S.-Y. Zhu, H. Namatame, M. Taniguchi, M.W. Haverkort, I.S. Elfimov, and A. Damascelli *Photoelectron Spin-Polarization Control in the Topological Insulator Bi2Se3.* Phys. Rev. Lett. **112**, 076802 (2014).

[24] J. Sánchez-Barriga, A. Varykhalov, J. Braun, S.-Y. Xu, N. Alidoust, O. Kornilov, J. Minár, K. Hummer, G. Springholz, G. Bauer, R. Schumann, L. V. Yashina, H. Ebert, M. Z. Hasan,and O. Rader *Photoemission of Bi_2Se_3 with Circularly Polarized Light: Probe of Spin Polarization or Means for Spin Manipulation?* Phys. Rev. X **4**, 011046 (2014).

[25] C-H. Park, and S. G. Louie, *Spin polarization of photoelectrons from topological insulators* Phys. Rev. Lett. **109**, 097601 (2012).

[26] Z. Gong, G.-B. Liu, H. Yu, D. Xiao, X. Cui, X. Xu, and W. Yao *Magnetoelectric effects and valley-controlled spin quantum gates in transition metal dichalcogenide bilayers* Nat. Comm. **4**, 2053 (2013).

[27] M. Gehlmann, Irene Aguilera, G. Bihlmayer, E. Młyńczak, M. Eschbach, S. Döring, P. Gospodarič, S. Cramm, B. Kardynał, L. Plucinski, S Blügel, and C. M. Schneider, *Quasi 2D electronic states with high spin-polarization in centrosymmetric MoS_2 bulk crystals* Scientific Reports **6**, 26197 (2016).

[28] For the case of normal incident linearly-polarized light all states with $m_k - m = 0, \pm 1$ are equally accessible, this result in $|\boldsymbol{\kappa}_{2,-2} \cdot \boldsymbol{\epsilon}_{p/s}| \approx |\boldsymbol{\kappa}_{2,2} \cdot \boldsymbol{\epsilon}_{p/s}|$, and a positive spin polarization is observable only when a disproportion of intensity from the two initial states is introduced by the IMFP.

[29] The P_z maps have been calculated according to the formulas $P = (I^{\uparrow} - I^{\downarrow})/(I^{\uparrow} + I^{\downarrow})$, $I^{\sigma} = I^{\sigma}(1) + I^{\sigma}(2)$, where the total photoemission intensity I^{σ} associated with a dipole transition to a final state of spin σ contains the contributions of the two degenerate initial states $I^{\sigma}(1)$ and $I^{\sigma}(2)$.

[30] In case of finite λ_e the magnitude of $I^{\uparrow}$ is similar for s, p, and C_L polarizations since it is mainly determined by the photoemission from the first layer. The magnitude of $I^{\downarrow}$ for C_R is reduced by a factor $\sim e^{-\frac{c}{2\lambda_e}}$, since it is mainly determined by the photoemission from the second layer.

[31] U. Heinzmann and J. Hugo Dil *Spin-orbit-induced photoelectron spin polarization in angle-resolved photoemission from both atomic and condensed matter targets*, J. Phys.: Condens. Matter **24** 173001, (2012).

[32] S.-K. Mo, C. Hwang, Y. Zhang, M. Fanciulli, S. Muff, J. H. Dil, Z.-X. Shen, and Z. Hussain *Spin-resolved photoemssion study of epitaxially grown $MoSe_2$ and WSe_2 thin films*, J. Phys.: Condens. Matter **28**, 454001 (2016).